# Compensation of Scanner Creep and Hysteresis for AFM Nanomanipulation

Babak Mokaberi *Student Member, IEEE*, and Aristides A. G. Requicha, *Life Fellow, IEEE*

***Abstract*—Nanomanipulation with Atomic Force Microscopes (AFMs) for nanoparticles with overall sizes on the order of 10 nm has been hampered in the past by the large spatial uncertainties encountered in tip positioning. This paper addresses the compensation of nonlinear effects of creep and hysteresis on the piezo scanners which drive most AFMs. Creep and hysteresis are modeled as the superposition of fundamental operators, and their inverse model is obtained by using the inversion properties of the Prandtl-Ishlinskii operator. Identification of the parameters in the forward model is achieved by a novel method that uses the topography of the sample and does not require position sensors. The identified parameters are used to compute the inverse model, which in turn serves to drive the AFM in an open-loop, feedforward scheme. Experimental results show that this approach effectively reduces the spatial uncertainties associated with creep and hysteresis, and supports automated, computer-controlled manipulation operations that otherwise would fail.**

***Note to Practitioners*—Manipulation at the nanoscale by using Atomic Force Microscopes (AFMs) as sensory robots is well established in research laboratories, and has great potential as a process for prototyping nanodevices and systems, for repairing structures built by other means, and for small batch manufacturing by using multi-tip arrays. However, precise (to ~ 1 nm, say) AFM nanomanipulation is currently very labor intensive, primarily because of the uncertainty in the position of the AFM tip relative to the sample being manipulated. Positional errors are due to thermal drift and various nonlinearities exhibited by the piezoelectric scanners used by most AFMs. This paper describes a technique for compensating creep and hysteresis, which, after drift, are the major causes of spatial uncertainty in AFMs. The compensator introduced here has been tested experimentally and shown to reduce creep and hysteresis effects by more than an order of magnitude. The creep and hysteresis compensator in this paper, together with the drift compensation scheme discussed in an earlier paper by the authors, provide means to reduce spatial uncertainties to a level that enables automatic manipulation, without a user in the loop, and therefore promise to greatly increase the throughput and accuracy of nanomanipulation operations.**

***Index Terms*—Atomic Force Microscopes; AFMs; automatic nanomanipulation; creep; hysteresis; nanolithography; nanomanipulation; nanorobotics; nonlinearities; Scanning Probe Microscopes; SPMs; spatial uncertainty.**

Manuscript received November 23, 2005. This work was supported in part by the NSF under grants EIA-98-71775 and DMI-02-09678.

B. Mokaberi is with the Laboratory for Molecular Robotics, 941 Bloom Walk, University of Southern California, Los Angeles, CA 90089-0781 (e-mail: mokaberi@usc.edu).

A. A. G. Requicha is with the Laboratory for Molecular Robotics, 941 Bloom Walk, University of Southern California, Los Angeles, CA 90089-0781 (tel: 213.740.4502; fax: 213.740.7512; e-mail: requicha@usc.edu).

## I. Introduction

NANOMANIPULATION with Atomic Force Microscopes (AFMs) is a relatively well established technology, which has been under development for over a decade—see e.g. [1], [2] and references therein. It has potential applications in device prototyping (for design validation, parameter optimization and sensitivity studies), repair of structures built by other means, building of templates such as stamps or molds, and for small batch fabrication by using multi-tip arrays. Its primary drawback is its low throughput. This can be combatted by parallelism (using multi-tip arrays as noted above) and by automation, which bypasses the time-consuming and labor-intensive interactive process that is typically used today to manipulate objects with overall dimensions on the order of 10 nm or less.

There are many problems that arise in successfully automating nanomanipulation, ranging from sample preparation to real-time feedback. However, in our experience over the last decade we have found that the most pernicious of these are the spatial uncertainties associated with the motion of the AFM tip. The most fundamental robotic tasks, “Go to point A” and “Move in straight line from point A to point B”, typically have not been implemented with sufficient accuracy for automated operation. A user in the loop has been needed to find the position of the tip relative to the particles or other objects being moved, to determine if a move was successful, and so on. This requires extensive imaging and is very time consuming. In addition, a user is normally forced to specify positions in pixel coordinates on the screen, and often this is not sufficiently accurate to ensure successful manipulation to the goal position.

An AFM motion in the horizontal plane of the sample is commanded by applying voltages to the instrument’s piezoelectric drive motors. In a traditional mobile robot, the odometry signal does not reliably measure the robot’s position. A similar situation arises in an AFM: the applied voltage signals are unreliable indicators of the tip’s position. The discrepancies in the AFM case are due to drift, creep, hysteresis and other nonlinearities inherent in the piezos and overall system. In our experience, drift is the major cause of spatial errors for AFM operation in ambient air and at room temperature. Drift compensation was addressed in [3], [4]. Now we focus on

creep and hysteresis, which are the next major culprits. (We ignore other nonlinearities because vendors' software and hardware usually compensate for them adequately.) Note that compensation must apply to "random", arbitrary trajectories to be useful for nanomanipulation; compensation only for the forward and backward motions needed for scanning is insufficient.

Several authors have studied the modeling and control of piezo actuators for accurate and fast positioning applications in Scanning Probe Microscopes (SPMs) [5]-[13]. For fast positioning, the higher vibrational modes of a piezo actuator are a crucial factor (typically at speeds above ~10 Hz). The vibrational modes of a scanner are modeled with a linear system [5], [7] and an optimal inverse controller is designed for regulating the desired output trajectory. In these cases an inverse feedforward controller is typically preferred over a feedback system due to the lack of positioning sensors or their low performance at high scanning speeds [6], [7]. In contrast, in nanomanipulation applications the scanner typically works at low speeds, on the order of 1 μm/s, and frequencies under ~10 Hz. Therefore the higher-frequency vibrational modes can be ignored, although the positioning accuracy is still substantially influenced by the creep and hysteresis effects.

Different methods have been suggested for eliminating the effects of creep and hysteresis in piezo actuators. In [8] a charge-based controller is proposed, and in [9] a capacitor is added in series to the piezo actuator. These methods typically add more drift to the scanner and significantly reduce the course of piezo movement. In a recent work [10] these problems are addressed by utilizing a charge amplifier. Although these methods can be effective in reducing creep and hysteresis, they require modifications to the existing hardware.

In [6] a cascade model for creep, hysteresis and vibrational dynamics of the piezo scanners is introduced, and the inverse dynamic is utilized to compensate for these effects in an open-loop fashion. In this work each effect is identified separately using an optical sensor for each of the $x$ and $y$ directions. In [11] a systematic approach for designing an $H_\infty$ controller for high bandwidth and high resolution positioning of piezo stack actuators is adopted. This work exploits high precision LVDT (Linear Variable Differential Transformer) sensors and reduces the nonlinear effects to ~ 65 nm (0.14%).

While in many works such as [7], [11] a linear nominal model is assumed for the piezo actuator and the existing nonlinearities are dealt with as uncertainties, a wide range of research has approached hysteresis as a non-local memory effect (see II.B for the definition) and tried to parametrically model it [6], [12], [13], [17]-[19]. Hysteresis can be observed in such systems and materials as mechanical structures, ferromagnetic materials and piezoelectric ceramics. The two distinct characteristics of hysteresis, i.e., the memory effect and the occurrence of hysteresis loops, make it a genuinely nonlinear phenomenon. In the early seventies a group of Russian scientists developed a new technique to model hysteresis based on a superposition of elementary hysteresis carriers called hysterons [14]. Since then, many mathematicians have contributed to the theory, and the important monographs of Mayergoyz [15] and Visintin [16] have appeared.

The early research on the hysteresis of actuators is based on the Preisach model [17], [18]. It uses a fundamental Preisach operator and approximates the hysteresis of a system with a weighted sum of fundamental operators. This model is computationally expensive, and cannot be extended to account for creep in a straightforward manner for piezoelectric materials. A better approach is to consider both creep and hysteresis in a single model by using the Prandtl-Ishlinskii (PI) operator [19]. The idea here is again to employ a superposition of several fundamental operators, now called play operators. PI modeling is used in this paper because it has several advantages over its Preisach counterpart: it is better suited to piezoelectric materials, it is easily extended to include creep, and the PI operator has a unique inverse.

The emphasis in this article is on the compensation of the spatial uncertainties associated with AFM creep and hysteresis for precise nanomanipulation. We introduce a new method for the identification of these effects using only information from the topography of a defined pattern on the surface—a nanoparticle pattern in our case. This method can be applied to the vast majority of AFM scanners in use today, where either there are no lateral positioning sensors or the accuracy of the sensors is insufficient. Moreover, the identification method can be applied to the scanner regularly (to take into account aging or environmental changes of piezo scanner dynamics) without needing any additional hardware for sensing the scanner's lateral movement. In essence, we use the SPM itself as its own lateral sensor, and we are limited primarily by the accuracy with which the SPM can measure features. This accuracy can be very high because SPMs can measure atomic and molecular features. The identified model is employed in an inverse-based feedforward compensator. Combining the creep and hysteresis compensator described here with the drift compensator introduced in [3], [4] yields a software-compensated AFM platform for precise nanomanipulation.

The remainder of the paper is organized as follows. Section II addresses the characteristics of the creep and hysteresis nonlinearities. In Section III, a nonlinear model is introduced, followed by a discussion of the inverse model and of an identification method. A topography-based estimation technique is presented in Section IV. The implementation and experimental results are described in Section V, and conclusions are drawn in the last section.

## II. Characteristics of Piezo Scanner's Nonlinearities

### A. Creep

When an abrupt change in voltage is applied to the scanner, the corresponding piezo dimensional change occurs in two stages: the first stage takes place in less than a millisecond, whereas the second one has a much longer time scale (see Figure 3.a). The second stage is known as creep.

Figure 1 demonstrates the effect of creep. A voltage step corresponding to a 1,000 nm displacement was applied to the

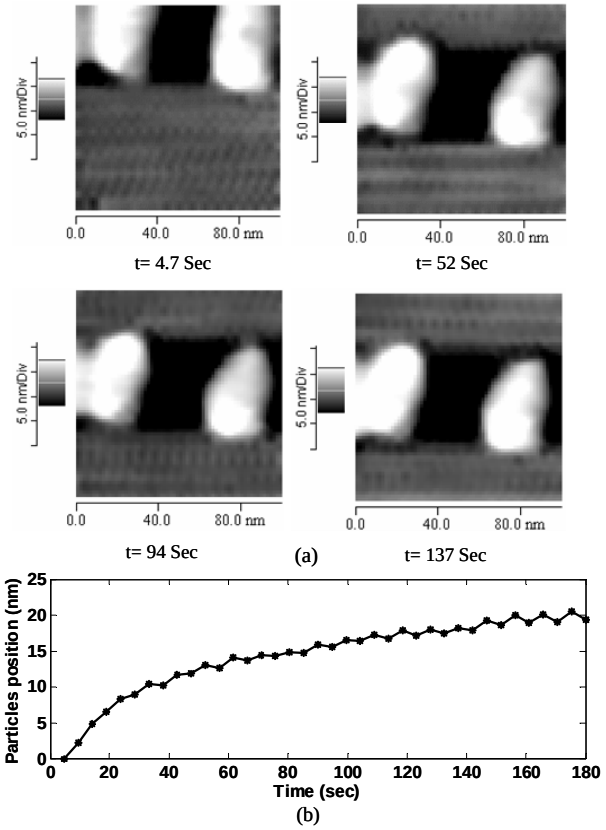


Fig. 1. (a) Successive images taken after a 1,000 nm step was applied to the scanner in the *y* direction. The scan size is 64x64 pixels, 100x100 nm, and the scanning speed 18 Hz. Due to the high speed scan the turnover effect of the tip appears as an artifact at the left side of the images. The horizontal "bands" in the image are an artifact of the flattening process used in imaging. (b) Changes in the *y* position of the particles for 180 sec. The observed ripples in the curve are attributed to hysteresis because we alternately scan upward and downward in the slow scan *Y* direction.

scanner, and then successive images were recorded around the (nominal) end position. (All the nanoparticle images in this paper were obtained in tapping mode with a Veeco AutoProbe CP-R with a 5μm scanner; fast scanning was in the *X* direction and slow scanning in *Y*. The images are of gold nanoparticles, with a nominal diameter 15 nm, on a mica surface coated with poly-L-lysine.) The particles in the successive images appear to be moving, although in reality the particles are fixed relative to the substrate. The tip, however, is still moving slowly ("creeping") after the 1,000 nm motion. An AFM image is built by assembling successive line scans, with each line being a plot of the height of the sample (typically measured by the voltage applied to the vertical piezo to keep the tip in contact with the sample) versus the voltage applied to the horizontal piezos. Therefore, when the tip is creeping the image appears to be moving. Creep effects can be noticeable for as much as 20% of the total length of the motion, and can last several minutes.

Quantitatively, the amount of creep can be expressed as the ratio of the second dimensional change to the first one. Typical values for the creep ratio are from 1% to 20%, and from 10 to 100 seconds for the phenomenon's time duration. In addition, the creep also manifests itself as a rate-dependent effect

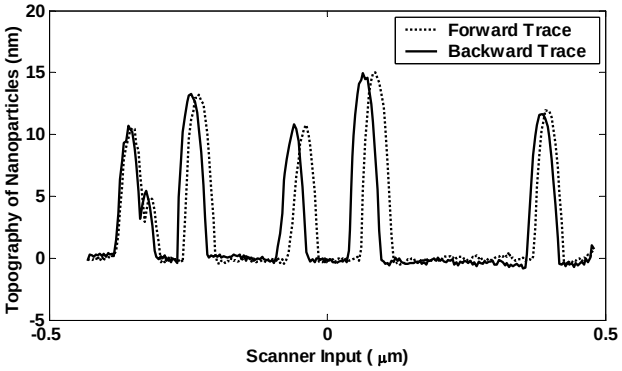


Fig. 2. Forward and backward traces over a set of 15 nm Au particles on mica. The length of the scan is 910 nm and the speed 2Hz.

when the scanner is driven by triangular and other input waveforms rather than by a step function.

### *B. Hysteresis*

Figure 2 illustrates the effect of hysteresis. A single line scan of a set of particles shows the particles in different positions, depending on whether the scan is in the forward or backward directions. Again, the effects can be large. In both Figure 1 and Figure 2 the motions occur within a few seconds and the effects of drift are negligible. Thus, even in a drift-compensated AFM, creep and hysteresis cause spatial uncertainties that are well beyond the threshold accuracy of a few nm that in our experiments we have found necessary for the successful manipulation of particles with sizes on the order of 10 nm.

Hysteresis in piezoelectric scanners is a non-local memory effect [15]. This means that the future values of the hysteresis output $f(t)$ for $t \geq t_0$ depend not only on the current value of the output $f(t_0)$ but also on the past extremal values of the input signal as well, i.e., on the points at which the input changes from increasing to decreasing and vice versa.

The amount of hysteresis in a piezoelectric scanner is defined as the ratio of the maximum divergence between the ascending and descending curves to the maximum extension that a voltage can create in the scanner (see Figure 3.b). Hysteresis effects can be as high as 15% in piezoelectric scanners. In addition, because of creep, a rate dependent effect may be observed in the hysteresis loops.

## III. MODELING OF SCANNER CREEP AND HYSTERESIS

### *A. Forward Model*

Creep can be modeled as a linear combination of several fundamental creep operators plus a term proportional to the input, to account for sudden changes in the output, as in Figure 3.a. Each creep operator is defined as a linear first order system

$$\frac{1}{\lambda_i}\dot{x}_i(t) + x_i(t) = u(t) \qquad (1)$$

with the poles located at $-\lambda_i < 0$ for $i = 1,2,...,N_c$ where $N_c$ represents the order of the creep model and $u(t)$ is the input

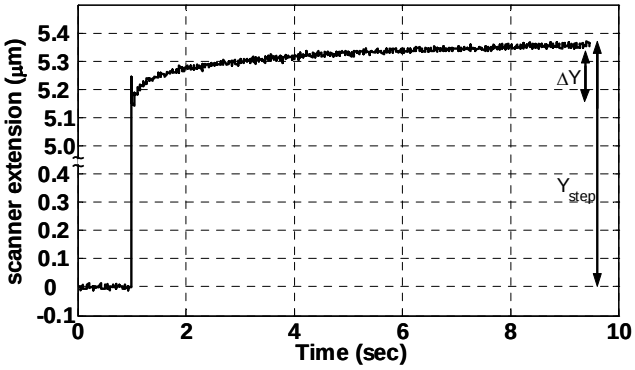


(a)

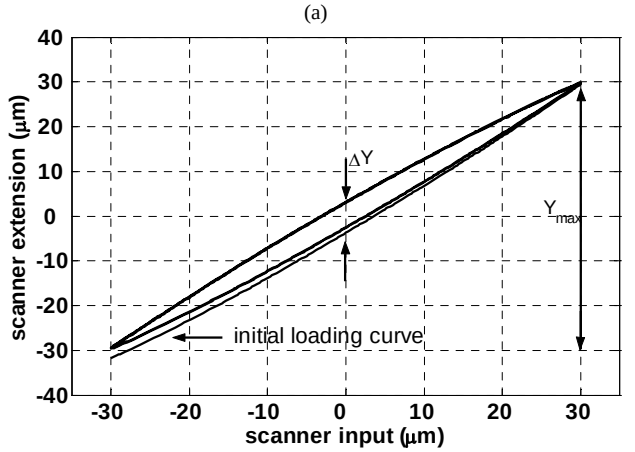


(b)

Fig. 3. (a) The creep effect observed from the scanner response to a 5.4 μm step function. (b) Hysteresis effect due to a triangular waveform. The scanner initially traverses a loading curve and after a few cycles it approaches a stable hysteresis loop. This initial behavior is observed every time the scanner takes a different starting point for a cyclic movement. These data were acquired on a 100 μm scanner with a positioning sensor with RMS noise level of about 15 nm, which is not sufficient for accurate nanomanipulation.

signal to the scanner. Thus, the discrete model of creep, assuming sampling period $T$, can be represented in the following state-space form:

$$\begin{aligned} x_i(k) &= e^{-\lambda_i T} x_i(k-1) + (1-e^{-\lambda_i T})u(k-1) \\ y_C(k) &= \sum_{i=1}^{N_c} c_i x_i(k) + au(k) \qquad c_i \geq 0 \end{aligned} \tag{2}.$$

Here the $x_i$ denote the creep operator states and $y_C$ the output. Hysteresis is modeled by using a similar idea, but with a nonlinear rate-independent fundamental operator called *play operator*. The input-output behavior of a play operator with a threshold value $r > 0$ is given by the hysteresis diagram depicted in Figure 4.a.

To define the play operator mathematically we need to divide the input trajectory into a set of monotone intervals (see Figure 4.b), where in each interval $t_i < t \leq t_{i+1}$ *(i=0,1,..N-1)*, $u(t)$ is either monotonically increasing or decreasing. In Figure 4.a the top horizontal part of the loop corresponds to the value $z_r(t_i)$ when the input stops increasing and starts decreasing. Similarly, the lower horizontal part corresponds to $z_r(t_i)$ when the input stops decreasing and starts increasing. While $u$ increases, $z_r(t) = \max\{z_r(t_i), u - r\}$, and while $u$ decreases, we

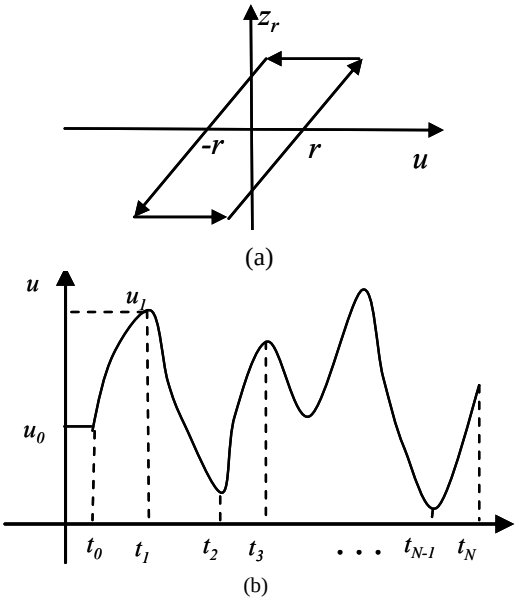


(a)

(b)

Fig. 4. (a) Input-output behavior of a *play operator* with threshold $r$. (b) Dividing the input waveform into a set of monotone intervals.

have $z_r(t) = \min\{z_r(t_i), u + r\}$. These two expressions can be combined to define the output of a play operator as

$$z_r(t) = \max\{u(t) - r, \min\{z_r(t_i), u(t) + r\}\} \quad \text{for } t_i < t \leq t_{i+1} \tag{3}.$$

In the discrete-time domain, the corresponding expression is

$$z_r(k) = \max\{u(k) - r, \min\{z_r(k-1), u(k) + r\}\} \tag{4}.$$

Alternatively, we can write:

$$\begin{aligned} &z_r(k-1) \geq u(k) + r \Rightarrow z_r(k) = u(k) + r \\ &z_r(k-1) \leq u(k) - r \Rightarrow z_r(k) = u(k) - r \\ &u(k) - r < z_r(k-1) < u(k) + r \Rightarrow z_r(k) = z_r(k-1) \end{aligned} \tag{5}.$$

The model approximates the behavior of the hysteresis in the piezo scanner by the superposition of a sufficiently large number of play operators:

$$y_H(k) = \sum_{i=1}^{N_H} w_i z_{r_i}(k) \tag{6}$$

where $N_H$ is the order of the hysteresis model, and $w_i > 0$ are the weights associated with the play operators.

By adding (2) and (6), the overall extension of the scanner can be defined as the sum of two terms,

$$y(k) = y_C(k) + y_H(k) = \underbrace{\sum_{i=1}^{N_c} c_i x_i(k)}_{L[u](k)} + \underbrace{au(k) + \sum_{i=1}^{N_H} w_i z_{r_i}(k)}_{P[u](k)} \tag{7}.$$

The first term, $L[u](k)$ is a rate-dependent term which depends on the past values of the input through the $x_i$ terms in (2), and the second term, called a Prandtl-Ishlinskii (PI) operator, is a rate-independent term which depends on the *current* values of the input.

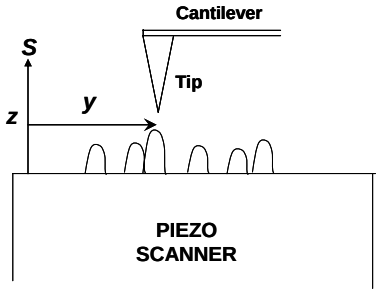


Fig. 5. The piezo scanner can move in any of the 3 dimensions. The scanner's vertical extension is controlled by a separate circuitry, which keeps the tip at a fixed distance from the surface of the sample. The horizontal movement of the piezo scanner is measured as the distance between the fixed coordinate system *S* on the scanner and the AFM's tip.

### *B. Inverse Model*

The hysteresis characteristics of the PI operator are completely defined by the so-called *initial loading curve*. It is a special branch traversed by $P_I[u](k)$ when driven by a monotonically increasing input with its state initialized to zero (i.e., $z_{r_i}(0) = 0$). The initial loading curve is defined through the weighting values $w_i$ and the threshold values $r_i$ as

$$\varphi(r) = \sum_{j=0}^{i} w_j (r - r_j) \quad r_i \le r < r_{i+1}, i = 0,1,...,N_H \tag{8}$$

where $w_0 = a$, $r_{N_H+1} = +\infty$ and $r_0 = 0$.

In [19], [20] it is proved that the PI operator is piecewise continuous and invertible, and its inverse is also a PI operator expressed as

$$P_I^{-1}[v](k) = \hat{a}v(k) + \sum_{i=1}^{N_H} \hat{w}_i z_{\hat{r}_i}(k) \tag{9}$$

with the parameters $\hat{a}$, $\hat{w}_i$ and $\hat{r}_i$ defined by

$$\hat{a} = 1/a$$

$$\hat{r}_i = \varphi(r_i) = \sum_{j=0}^{i} w_j (r_i - r_j) \quad i = 0,1,...,N_H \tag{10}.$$

$$\hat{w}_i = \frac{-w_i}{(a + \sum_{j=1}^{i} w_j)(a + \sum_{j=1}^{i-1} w_j)} \quad i = 1,2,...,N_H$$

In [19] it is also shown that for every continuous input signal, the PI operator is Liptschitz continuous and causally invertible as long as the *generator function* $\varphi(r)$ is monotically increasing (which is satisfied if $a, w_i, r_i > 0$ for $i=1,2,\ldots,N_H$). This means that, under the above condition, for every continuous function $v$ there exist a unique input function $u$ such that

$$u(k) = P_I^{-1}[v](k) \tag{11}.$$

We always assume piecewise continuous functions for the output trajectory and use positive parameters that ensure that $\varphi(r)$ is monotonically increasing. Denote the desired output trajectory of the scanner by $y_d(k)$ and replace it in the left side of (7). We can rewrite (7) as

$$y_d(k) - L[u](k) = P_I[u](k) \tag{12}.$$

To solve this equation for $u$ we let

$$v(k) = y_d(k) - L[u](k) \tag{13}$$

and apply the inverse PI operator (11) to $v$. Although $v$ depends on $u$, we can apply the previous equations recursively to find the input $u$ that corresponds to the desired output $y_d$. We proceed as follows. Given all the forward model parameters in (2) and (6)—see below how these parameter values are identified—we compute the inverse model parameters per (10). Next we compute $x_i(k)$ by using (2) and therefore obtain $L[u](k)$. Observe that the expression for $x_i(k)$ in (2) uses only the previous values of the input, $u(k\text{-}1)$, and these are available from the recursion. Subtraction from $y_d(k)$ yields $v(k)$, per (13). Now we need to apply the inverse PI operator to $v$. To do this we compute the relevant $z_r(k)$ values by applying (4) with $u$ replaced by $v$, and plug the results into (9). Per (11), the result is the $u(k)$ that will produce the desired output when fed as input to the scanner.

### *C. Estimation of Scanner's Model Parameters*

Assume that there is a sample firmly attached to the scanner, such that neither the sample nor the deposited material on the sample (nanoparticles, say) is sliding with respect to each other (Figure 5). For simplicity assume that the scanner moves horizontally in only one direction. The topography of the sample is measured with respect to a fixed coordinate system $S$ attached to the top of the scanner. If the extension of the scanner is zero, the AFM's tip always remains at a distance $y_0$ with respect to $S$, assuming that the effect of drift has been eliminated. This argument is true even when the cantilever and the tip are oscillating vertically (for example, in tapping mode).

The scanner extends by $\Delta y$ when a voltage is applied to it, and the position of the tip with respect to the coordinate system $S$ is simply $y = y_0 + \Delta y$. (For simplicity of the equations $\Delta y$ is assumed positive when the scanner extends to the left in Figure 5.) Along the line that is being scanned, the sample topography can be characterized by the function $h(y)$, where $h$ is the height of the sample. Note that the height $h$ can be measured very accurately by the AFM, but the true extension $y$ of the piezo is unknown; what is known is the input voltage $u$ to the actuator. Estimation of the function $h(.)$ is discussed below, in Section IV, and involves finding the relationship between piezo extension and input voltage. For now, we assume that $h(.)$ is a known function.

The overall dynamics of the scanner can be represented by the following expression,

$$\begin{cases} y(k) = y_0 + au(k) + \sum_{i=1}^{N_c} c_i x_i(k) + \sum_{i=1}^{N_H} w_i z_{r_i}(k) \\ z_m(k) = h(y(k)) \end{cases} \tag{14}.$$

Here $z_m(k)$ denotes the height of the sample measured by the

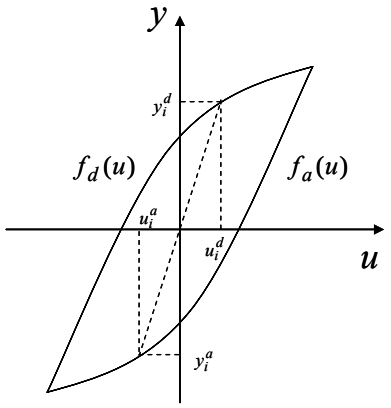


Fig. 6. A typical hysteresis loop with the natural symmetry around the zero field.

AFM at time instant *k*.

The identification parameters can be lumped together in the vector $\theta$ as

$$\theta = \begin{bmatrix} c_i & e^{-\lambda_i T} & a & w_j & r_j & y_0 \end{bmatrix}^T, i = 1,..,N_c \text{ , } j = 1,..,N_H \quad (15).$$

There are $2N_c + 2N_H + 2$ parameters to be identified.

Since the model is highly nonlinear and may have numerous local minima, we use a Recursive Least Square algorithm (RLS) with a covariance resetting scheme [21], [22]. The behavior of the system output is predicted based on the current estimates of the parameters. The predictor is simply the model in (14) using the current estimates of the parameters. We denote by $\hat{y}(k)$ the value of *y* computed by (14) using the parameter estimates $\hat{\theta}(k-1)$. The predicted output is

$$\hat{z}_m = h(\hat{y}(k)) . \quad (16)$$

The prediction error is defined as the difference between the measured and the predicted output

$$\varepsilon(k,\theta) = z_m(k) - h(\hat{y}(k)) . \quad (17)$$

The gradient of the prediction error with respect to each parameter is used as the regressor. It is a vector with the same dimension as $\theta$ and computed by

$$\psi(k,\theta) = \left[ -\frac{\partial \varepsilon(k,\theta)}{\partial \theta} \right]^T = \frac{\partial h(\hat{y}(k))}{\partial \hat{y}} \cdot \left[ \frac{\partial \hat{y}(k)}{\partial \theta} \right]^T . \quad (18)$$

Here a derivative with respect to $\theta$ is shorthand for a vector whose components are the derivatives with respect to the various parameters in $\theta$.

Since the function *h*(.) is known, its gradient is also known. Most of the components of the vector $\partial \hat{y}(k) / \partial \theta$ can be easily derived from (2) and (14). The derivatives with respect to the hysteresis thresholds are more complicated but can be computed by using (5):

$$\partial \hat{y}(k) / \partial r_i = \begin{cases} \hat{w}_i & \text{if } z_{r_i}(k-1) - \hat{r}_i \geq u(k) \\ \dfrac{\partial \hat{y}(k-1)}{\partial r_i} & \text{if } z_{r_i}(k-1) - \hat{r}_i < u(k) < z_{r_i}(k-1) + \hat{r}_i \\ -\hat{w}_i & \text{if } z_{r_i}(k-1) + \hat{r}_i \leq u(k) \end{cases} \quad (19).$$

Note that the values at time $k-1$ of the various variables in (19) are available from the recursion.

In the RLS algorithm, the information from the input signal to the scanner $u(k)$, and the measured topography $z_m(k)$ are used recursively to estimate the parameters in $\theta$.The algorithm can be summarized as [22]

$$\hat{\theta}(k) = \hat{\theta}(k-1) + \frac{\alpha(k) P(k-1) \psi(k)}{1 + \alpha(k) \psi^T(k) P(k-1) \psi(k)} . \varepsilon(k, \hat{\theta}(k-1))$$

$$P(k) = P(k-1) - \frac{\alpha(k) P(k-1) \psi(k) \psi^T(k) P(k-1)}{1 + \alpha(k) \psi^T(k) P(k-1) \psi(k)} \quad (20)$$

$$\alpha(k) = \begin{cases} \dfrac{\psi^T(k) P(k-1) \psi(k)}{\psi^T(k) \psi(k)} & \text{if } \psi^T(k) \psi(k) \neq 0 \\ 1 & \text{otherwise} \end{cases}$$

In these equations, $P$ denotes the covariance of the parameter estimates and $\psi(k) = \psi(k, \hat{\theta}(k-1))$.

When the minimum eigenvalue of the covariance matrix $P(k)$ becomes very small, we reset the covariance to a large number $P(k) = p_0 I$. This action is typically done with a period $k_0$, and prevents the identified parameter from getting stuck at a local minimum.

## IV. Estimation of the Hysteresis Cycle

Knowledge of the function $h(\cdot)$ is crucial for the identification process described in the previous section. If we move the tip along a specific line between two extrema, the AFM measures the height of the sample *as a function of input voltage u* along the line. However, the identification algorithms need the height as a function of the scanner extension *y*, not of the input *u*. The required *h*(*y*) can be estimated if we determine the relationship between *u* and *y* that applies along the selected scan line. This can be done as follows.

We use a sample in which gold nanoparticles are deposited on a mica substrate coated with poly-L-lysine. Because of their nearly exact spherical shape, there are certain features of the nanoparticles that do not change during the scans and can be used to localize the scanner horizontally. These features are a particle's center, or its peak height on a vertical plane that contains the scan line.

Figure 2 shows two scans of such a sample, one in the forward and the other in the backward direction along the same line. The effect of the scanner's dynamics is apparent as a mismatch between the forward and backward traces. If all the nonlinearities in the scanner were compensated, then not only the forward and backward traces would coincide, but also all other input waveforms would produce the same topography.

To relate input voltage to piezo extension we exploit the symmetry of a steady-state hysteresis loop [20], in which the effects of the initial loading curve are negligible. We divide a hysteresis loop into an ascending (forward) and a descending (backward) curves (Figure 6). These curves can be represented by a set of points $(u_i^a, y_i^a)$ in the ascending curve and

the corresponding symmetric pairs $(u_i^d, y_i^d)$ in the descending curve. The hysteresis loop in piezo materials is rotationally symmetric about the zero field (where the applied voltage to the scanner is equal to zero). If we call the center of symmetry $(u^s, y^s)$ (which has been assumed to be zero in Figure 6) then we have

$$\begin{cases} 2u^s = u_i^a + u_i^d \\ 2y^s = y_i^a + y_i^d \end{cases} \quad \text{for } i = 1,2,....,N \ . \tag{21}$$

Therefore, if we define $f_a(u)$ as the ascending function, the descending part satisfies

$$f_d(u) = 2y^s - f_a(2u^s - u) \ . \tag{22}$$

In practice, the function $f_a(u)$ is well approximated by a polynomial with degree $\geq 5$.

Because of this relationship between the ascending and descending curves it is possible to estimate them using the information from the particles' peaks in Figure 2. For each particle, the peaks in the forward and backward traces correspond to the same extension of the piezo scanner. Therefore, if we call the horizontal coordinates of these peaks in the forward and backward traces $u^a$ and $u^d$, respectively, then we have $f_d(u^d) = f_a(u^a)$, which, together with (22) can be written as

$$f_a(u^a) + f_a(2u^s - u^d) = 2y^s \tag{23}.$$

Assuming we have *n* particles in Figure 2, we will generate *n* equations from (23). This set of equations, together with an additional condition on the vertical scale of Figure 2, can be used in a least-squares fitting algorithm to find the coefficients of a polynomial approximation to $f_a(u)$. The vertical scale is related to the calibration of the scanner and is normally set such that $f_a(u_{\max}) - f_a(u_{\min}) = u_{\max} - u_{\min}$. Once the function $f_a(u)$ is computed, we can replace the values of *u* in the forward scan shown in Figure 2 by the corresponding values of *y* obtained by inverting $f_a(u)$. This is the desired *h*(*y*) function for the forward scan trajectory. Note that we have found a polynomial approximation for the hysteresis loop for a specific input waveform, but this cannot be used for arbitrary input signals.

## V. Implementation and Experimental Results

The procedure for the compensation of creep and hysteresis involves the following steps. (For simplicity of exposition, we consider only one of the principal directions, *X*, say.)

1) Select a working area (1x1μm, say) and choose a line in the *X* direction that crosses a number of particles greater than the polynomial order of $f_a(u)$. The line should span the entire region in which manipulation operations will take place.

2) Perform a few cycles of single line scans over the particles along the selected line. Once the cycles are stable, estimate $f_a(u)$ and *h*(*y*) using the procedure in Section IV.

3) Scan along the same line with an input similar to that in Figure 7.a and record the measured heights $z_m(k)$ and input signals $u(k)$. Use this information to recursively estimate the forward model parameters $\theta$, by using the algorithms in Section III.C.

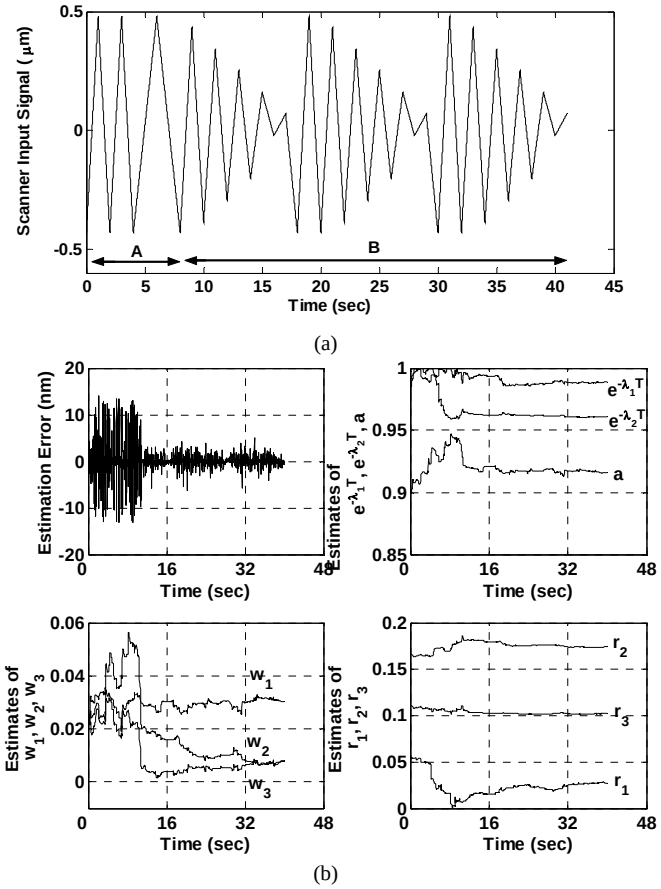


Fig. 7. (a) The input waveform used to estimate *h*(.), interval **A**, and to estimate the parameters of the model, interval **B**. (b) The estimation error and several parameter estimates as functions of time in the computation.

4) Compute the inverse model parameters from (10), Section III.B.

5) Now, for any desired output trajectory $y_d(k)$, use the inversion procedure of Section III.B to find the required input signal $u(k)$ and apply it to the scanner.

The recursive estimation procedures used in the approach just outlined require initial values, and it is not clear how to set them. We found experimentally that setting all initial conditions to zero and running a few large cycles initializes the system adequately and produces good results.

In our implementation we normally use the input waveform in Figure 7.a for system identification. This waveform excites all the fundamental operators in the dynamic model, since it causes the tip to move over the entire scan length. An order $n_c = 2$ for creep and $n_H = 8$ for hysteresis were selected on the basis of experimental results. Time was quantized with a *T*=8 msec sampling interval. The first part of the waveform, indicated by **A** in Figure 7.a, is used to produce a stable hysteresis loop in order to estimate the function $h(.)$, and the rest

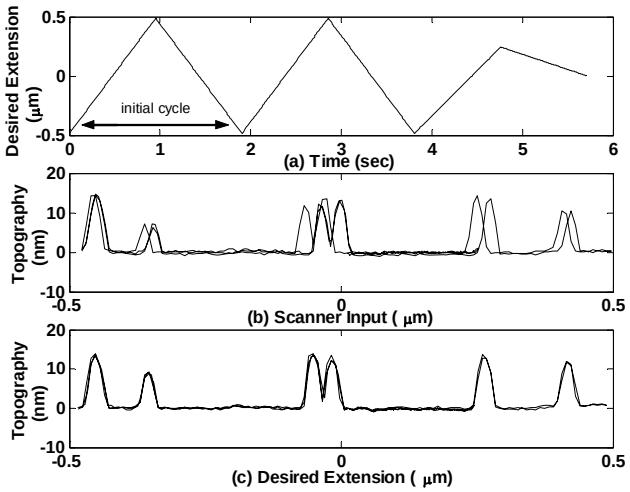


Fig. 8. (a) A desired trajectory, which corresponds to forward and backward motions along a line that intersects six particles. The initial cycle serves to adjust the initial conditions of the model. (b) The topography traces obtained by applying the desired trajectory directly as input to the scanner. (c) The topography of the sample versus the desired extension when the compensation procedure is applied.

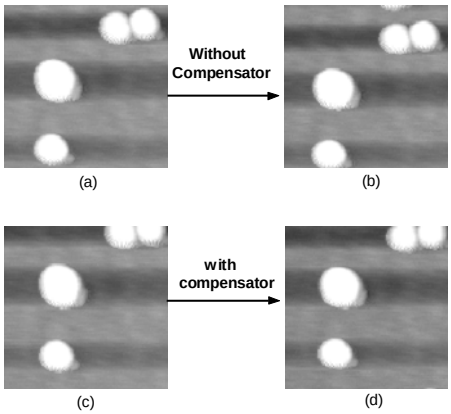


Fig. 9. The images are 253x253 nm scans of 15 nm Au particles. The initial images (a) and (c) were taken at the coordinates (0.3,0.3) micrometers. Then a sequence of tip movements was performed, visiting successively the points (0.3,0.3), (-0.5,-0.3), (0.45,0.45), (-0.4,-0.4) and (0.3,0.3). Thus, after traversing an arbitrary path, the AFM's tip is sent back to its initial position. The images (b) and (d) were taken at the final position of the tip immediately after the motion. Without the compensator there is a displacement of about 14.3 nm between (a) and (b), whereas with the compensator a displacement of about 1.0 nm is measured between (c) and (d).

of the input waveform, indicated by **B,** drives the parameter identification process. The estimation error (17) and several of the parameter estimates are depicted in Figure 7.b.

To test the algorithm in one dimension ($X$), we used the desired trajectory $y_d$ that is shown in Figure 8.a as the piezo extension as a function of time. First, we applied the desired trajectory directly as input to the scanner. The result is depicted in Figure 8.b as the measured height $z_m$ (the topography signal) versus the input signal, which in this case equals the desired extension $y_d$. Observe that several distinct topography traces are obtained because of the scanner nonlinearities. Each trace corresponds to one of the ascending or descending ramps in the input waveform.

Next we applied the compensation procedure. The first large cycle in the $y_d$ waveform serves to set the initial conditions in the recursion calculations. Then from time about 1.9 sec, the trajectory $y_d$ is used in the inversion procedure of Section III.B to compute the input signal $u$ that generates the desired scanner's extension waveform. The results are shown in Figure 8.c: the measured topography signals (versus the desired extension) that correspond to the various forward and backward motions prescribed in the waveform of Figure 8.a are nearly indistinguishable. This shows that the compensator is working very well.

For two-dimensional motions of the tip, we assume a negligible coupling between the dynamics in $X$ and $Y$ and use an independent identification procedure for each of the directions. Given any trajectory in the plane, we project it on the orthogonal axes $X$ and $Y$, and apply the corresponding inverse models to determine the input signal to the scanner. Experiments show that this procedure generates good results.

To test the compensator in two dimensions, the AFM's tip performed a series of straight-line motions given in the caption of Figure 9. The path is defined in such a way that the starting and ending points have (nominally) the same coordinates: (0.3, 0.3) micrometers. Before starting the path, a 253x253 nm image was scanned, and at the end of the path another image with the same scan size was acquired. By comparing the initial and final images using the cross-correlation method described in [4], the translation between the 15 nm gold nanoparticle images was computed. In the uncompensated motion, there is a difference of about 14.3 nm between the starting point and the final position. This number was reduced to about 1.0 nm when we compensated for creep and hysteresis.

We ran a series of experiments to analyze the performance of the compensator in more detail. In these experiments the AFM scans two different areas, $A$ and $B$, each 117x117 nm in size. These areas are located at the distances $d$ from each other given in Table I. In each experiment the tip starts by scanning area $A$ and then moves to area $B$ in a series of "random" movements consisting of several straight line segments. Once the tip reaches the bottom-left corner of area $B$ it performs a scan in that area. After these two scans, the tip goes back to area $A$ and repeats the same sequence of scanning and random movements. At the end of each experiment four im-

TABLE I
STATISTICAL ANALYSIS OF COMPENSATOR

| $d$ (nm)[a] | Maximum Error without Compensator (nm)[b] | Maximum Error with Compensator (nm)[c] |
|---|---|---|
| 645 | 6.45 ± 0.17 | 0.76 ± 0.22 |
| 951 | 7.03 ± 0.84 | 0.78 ± 0.28 |
| 1150 | 9.53 ± 0.88 | 1.01 ± 0.19 |

[a] Distance $d$ is measured between the centers of area $A$ and $B$.
[b, c] Data are averaged over 5 different experiments. The paths between $A$ and $B$ are similar for all different rows but scaled according to the distance $d$.

ages are obtained, two from area *A* and two from area *B*. The scans in each area are cross-correlated and the differences between the scans are computed as the two-dimensional displacement between the particles. Table I shows the maximum errors averaged from 5 different experiments for each of the distances $d$. The table shows that the compensator reduces the errors roughly by an order of magnitude.

Figure 10 demonstrates the use of the compensator to manipulate 10 nanoparticles automatically (with no user in the loop) and form two five-particle structures that correspond to cells of a Quantum Cellular Automaton (QCA) [24]. Manipulation was performed as described in [1], [2], by moving along a line passing through the center of each particle and turning off the *Z* feedback. The particles were manipulated in the numeric order indicated in the left panel of the figure to maximize the distance that the tip travels between pushing operations, and therefore elicit large creep and hysteresis effects. Imaging was performed only before beginning the experiment and after all particles had been manipulated. In our experience, similar operations without the compensator fail most of the time.

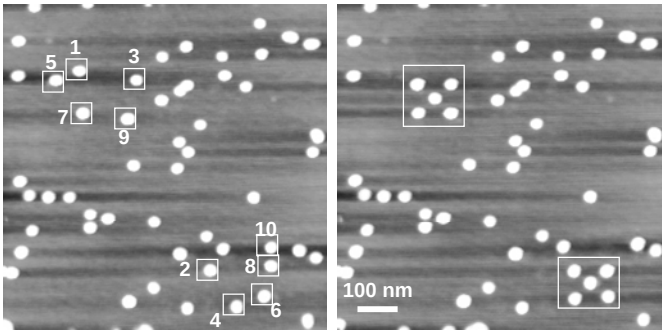


Fig. 10. Automatic manipulation of 10 gold nanoparticles to form two sets of Quantum Cellular Automaton (QCA) structures [24] in the compensated environment. The sequence of operations was chosen to force the AFM tip to travel between the two cells before pushing each particle. The compensated trajectory was used to accurately find the particles during the automatic manipulation. The whole process was performed twice, the first for coarse positioning and the second for accurately positioning the particles at the desired locations.

## VI. Conclusion

Creep and hysteresis are the major causes of spatial uncertainties in drift-compensated Atomic Force Microscopes (AFMs). In this paper we develop a joint model for scanner creep and hysteresis based on Prandtl-Ishlinskii (PI) operator techniques. The PI approach has advantages over the more traditional Preisach models: it can deal with both creep and hysteresis in an integrated fashion and PI operators have unique inverses.

We introduce a new, adaptive, recursive method for the identification of model parameters that uses solely information from the topography of the sample and is suitable for the identification of a large number of parameters. This method is applicable to the vast majority of the AFMs currently in use, which either have no sensors on the horizontal plane of the sample, or have feedback loops that are too noisy for nanomanipulation of small nanoparticles with overall sizes on the order of 10 nm. Our techniques are also applicable to other SPMs (Scanning Probe Microscopes) beyond AFMs, and are limited primarily by the SPMs' ability to measure small features. Because SPMs can reach atomic or molecular resolutions, the techniques described here can be extended to very small spatial scales.

The inverse model is used in an open-loop feedforward controller, which is shown experimentally to compensate effectively for creep and hysteresis. The same approach might also be used in the few of today's AFMs that have low-noise feedback loops, so as to increase the performance of their controllers, for example by using the inverse models developed here in feedforward components of their feedback systems.

The creep and hysteresis compensation techniques described here can be combined with their drift compensation counterparts introduced in [3], [4] to provide reliable implementations of the basic robotic primitive "Move from point A to point B", as demonstrated in this paper. In turn, this opens new possibilities in automatic nanomanipulation. High-level planning algorithms such as those in [23] driving a compensated AFM show promise of fully automatic operation. This will enable the construction of structures much more complex than those which can be built today.

This paper was primarily concerned with nanomanipulation operations, but it is important to point out that compensation of scanner nonlinearities is useful not only for nanomanipulation, but also for AFM-based nanolithography, and therefore may have wide applicability.

## Acknowledgment

The authors thank Professor Petros Ioannou, of USC's Electrical Engineering Department, for his helpful advice on control theory issues.

## References

[1] A. A. G. Requicha, "Nanorobots, NEMS and Nanoassembly", *Proc. IEEE*, vol. 91, no. 11, pp. 1922-1933, November 2003.

[2] A. A. G. Requicha, "Nanorobotics", in *Handbook of Industrial Robotics*, 2nd. ed, S. Nof, Ed., New York, NY: Wiley, 1999, pp. 199-210.

[3] B. Mokaberi and A. A. G. Requicha, "Towards automatic nanomanipulation: drift compensation in scanning probe microscopes*", Proc. IEEE Int'l Conf. on Robotics and Automation*, New Orleans, LA, pp. 416-421, April 25-30, 2004.

[4] B. Mokaberi and A. A. G. Requicha, "Drift Compensation for Automatic Nanomanipulation with Scanning Probe Microscopes ", *IEEE Transactions on Automation Science and Engineering,* vol. 3, no. 3, pp. 199-207, July 2006.

[5] Q. Zou and S. Devasia, "Preview-Based Optimal Inversion for Output Tracking: Application to Scanning Tunneling Microscopy", *IEEE Trans. on Control Sys. Tech.,* vol. 12, no. 3, pp. 375-386, May 2004.

[6] D. Croft, G. Shed and S. Devasia, "Creep, Hysteresis, and Vibration Compensation for Piezoactuators: Atomic Force Microscopy Application", *Journal of Dynamic Systems, Measurement, and Control,* vol. 123, pp 35-43, March 2001.

[7] G. Schitter and A. Stemmer, "Identification and Open-Loop Tracking Control of a Piezoelectric Tube Scanner for High-Speed Scanning-Probe Microscopy", *IEEE Trans. on Control Sys. Tech.,* vol. 12, no. 3, pp. 449-454, May 2004.

[8] M. Goldfarb and N. Celanovic, ‘‘Modeling piezoelectric stack actuators for control of micromanipulation’’ *IEEE Control Sys. Magazine,*, vol. 17, no. 3, pp 69-79, June 1997.
[9] H. Kaizuka ‘‘Application of capacitor insertion method to scanning tunneling microscopes,’’ *Rev. Sci. Instrum.*, vol. 60, no. 10, pp. 3119–3122, Oct. 1989.
[10] A.J. Fleming and S.O.R. Moheimani, “Sensorless Vibration Suppression and Scan Compensation for Piezoelectric Tube Nanopositioners”, *IEEE. Trans. on Control Sys. Tech.,* vol. 14, no. 1, pp. 33-44, Jan. 2006.
[11] S. Salapaka, A. Sebastian, J.P. Cleveland and M.V. Salapaka “High bandwidth nano-positioner: A robust control approach”, *Rev. Sci. Instrum.*, vol. 73, no. 9, pp 3232-3241, Sep 2002.
[12] P. Ge and M. Jouaneh “Tracking Control of a Piezoceramic Actuator” *IEEE Trans. on Control Sys. Tech.,* vol. 4, no 3, pp 209-216, May 1996.
[13] H. Jung, J. Shim and D. Gweon “Enhancement of AFM image by compensating the Hysteresis and Creep effect within PZT”, *Optical Eng. for Sensing and nanotech. (ICOSN’99),* vol. 3740, pp 327-330, June 1999.
[14] M.A. Krasnoselskii and A.V. Pokrovskii, *Systems with Hysteresis*. Heidelberg: Springer- Verlag, 1989.
[15] I.D. Mayergoyz, *Mathematical Models of Hysteresis*. New York, NY: Springer-Verlag, 1991.
[16] A. Visintin*, Differential Models of Hysteresis*. Berlin: Springer-Verlag, 1994.
[17] P. Ge and M. Jouaneh, “Generalized Priesach model for hysteresis nonlinearity of piezoceramic actuators”, *Precision Eng*., vol. 20, no. 2, pp. 99-111, April 1997.
[18] G. Berttoti, “Dynamic generalization of the scale Preisach model of hysteresis”, *IEEE Trans. Magn*., vol. 28, no. 5, pp. 2599-2601, Sep. 1992.
[19] P. Krejci and K. Kuhnen, “Inverse control of systems with hysteresis and creep”, *IEE Proc.-Control Theory Appl*., vol 148, no. 3, pp. 185-192, May 2001.
[20] M. Brokate and J. Sprekles, *Hysteresis and Phase Transitions*. New York, NY: Springer-Verlag, 1996.
[21] L. Ljung, *System Identification: Theory for the User*. Englewood Cliffs, NJ: Prentice Hall, 1998.
[22] P. Ioannou and J. Sun, *Robust Adaptive Control.* Englewood Cliffs, NJ: Prentice Hall, 1996.
[23] J. H. Makaliwe and A. A. G. Requicha, “Automatic planning of nanoparticle assembly tasks”, *Proc. IEEE Int'l Symp. on Assembly & Task Planning (ISATP ‘01)*, Fukuoka, Japan, pp. 288-293, May 28-30, 2001
[24] C. S. Lent et al., “Quantum cellular automata”, *Nanotechnology*, vol. 4, pp. 49-57, Jan. 1993.

**Babak Mokaberi** (S’05) received the B.S. degree from Isfahan University of Technology, Isfahan, Iran in 1995 and the M.S. degree from Sharif University of Technology, Tehran, Iran in 1998, both in Electrical Engineering. In 2001 he joined the University of Southern California, Los Angeles where he is currently a Ph.D. candidate in Electrical Engineering, at the Laboratory for Molecular Robotics. His research interests include dynamical system control of atomic force microscopes, automatic manipulation and assembly of nanostructures.

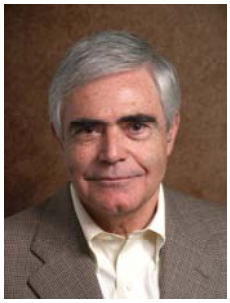

**Aristides A. G. Requicha** (Life Fellow, IEEE) was born in Monte Estoril, Portugal, in 1939. He received the Engenheiro Electrotécnico degree from the Instituto Superior Técnico, Lisbon, Portugal, in 1962, and the Ph.D. in electrical engineering from the University of Rochester, Rochester, NY in 1970. He was a college and high school Valedictorian.

He is currently the Gordon Marshall Professor of Computer Science and Electrical Engineering at the University of Southern California, where he also directs the Laboratory for Molecular Robotics. He has authored some 170 scientific papers, and has served in numerous conference program committees and journal editorial boards. His past research focused on geometric modeling of 3–D solid objects and spatial reasoning for intelligent engineering systems. Currently he is working on robotic manipulation of nanometer-scale objects using scanning probe microscopes; nanorobot components and nanorobotic system integration; fabrication of nanostructures by robotic self-assembly; sensor/actuator networks; and applications in NEMS (nanoelectromechanical systems) and nanobiotechnology. The long-term goals are to build, program, and deploy nanorobots and networks of nanoscale sensors/actuators for applications to the environment and health care.

Dr. Requicha currently is the editor-in-chief-elect of the IEEE Transactions on Nanotechnology and co-chairs the Micro and Nanorobotics Technical Committee of the IEEE Robotics and Automation Society. He is also a member of the AAAI, AAAS, AANM, ACM, AVS and SME. Personal web page: http://www-lmr.usc.edu/~requicha.